



The additional substitutions built into the last three sequences are intended to increase helicity: N-terminal acetylation, T4E, T6S, A8L, N14Q. The T4E substitution provides, on ionization, a carboxylate to stabilize the positive end of the helix macrodipole. These mutations also produce an LXXXLXXXL motif which could favor the formation of a longer amphiphilic  $\alpha$  helix. The U-series of peptides illustrated above share an identical seven residue C-terminal segment ending with  $-GY(NH_2)$ ; thus CD spectral differences should be readily quantifiable and uncomplicated by changes in the contribution of aromatic sidechain chromophores [18]. Herein we report CD and NMR comparisons for  $U_0$ ,  $U_1$  and  $U_5$ .

## 2. Materials and methods

### 2.1. Peptide preparation and quantitation

Amylin fragments [Ser<sup>2,7</sup>]-hAM(1–20)GNH<sub>2</sub>,  $U_0$ ,  $U_1$  and  $U_5$  were prepared at Amylin Pharmaceuticals Inc. by automated solid-phase peptide synthesis using standard Fmoc procedures, purified to  $\geq 94\%$  homogeneity (with no individual impurities present in NMR detectable quantities) by reverse phase gradient preparative HPLC (acetonitrile/0.1% aqueous TFA) and characterized by electrospray mass spectrometry. The NMR studies reported in part herein confirm the sequences. Aqueous peptide stock solutions (pH  $\leq 6$ ) were quantitated by UV:  $\epsilon_{274}-\epsilon_{310} = 1405$  [19] for systems lacking a disulfide linkage,  $\epsilon_{274}-\epsilon_{310} = 1555$  [16] when a disulfide is present.

### 2.2. Circular dichroism spectroscopy

CD spectra were recorded as previously described [9–11], using a JASCO model J720 spectropolarimeter, which had stabilized for at least 30 min with a nitrogen flow rate of 5 l/min, and which was frequently calibrated using the (+)-10-camphorsulfonic acid (CSA) sample provided by the JASCO. For the far UV range, we assume that the CSA minimum corresponds to  $[\theta]_{192.5} = -15\,600$  [1,20]. Final peptide concentrations of 20–60  $\mu$ M in the CD cells (1 or 2 mm path length) were obtained by quantitative serial dilution of the UV quantitated stock solutions. The aliquot of stock solution is added to a premixed v/v ratio of an aqueous buffer with the other components required (see below). The aqueous buffer used throughout was 10 mM acetate. The accumulated (16–24 scans) average spectra were trimmed at a photomultiplier voltage of 650 V and smoothed using the reverse Fourier transform procedure in the JASCO software prior to subtracting a similarly smoothed solvent baseline. All subsequent CD spectral values for peptides are expressed in units of residue molar ellipticity (deg·cm<sup>2</sup>/residue dmol); solvent compositions as volume % values, with the volume designation deleted. Thermal unfolding studies (at a peptide concentrations of circa 50  $\mu$ M) in the temperature range 268–353 K employed 50% aqueous ethylene glycol as the cryogen which was pumped through the metal block holding the cells; 20 min was allowed for thermal equilibration prior to recording each spectrum. The temperatures were read from a calibrated thermometer inserted in the cell block.

### 2.3. NMR spectroscopy

Spectra for qualitative structure definition were recorded for 2–4 mM peptide solutions (aqueous buffer, 20 mM acetate and 20 mM formate, pH 3.3  $\pm$  0.3, diluted with fluoroalcohol (hexafluoroisopropanol, HFIP, or trifluoroethanol, TFE) to the desired volume percent) at 500 MHz using previously described [9] protocols for TOCSY, COSY, ROESY and NOESY experiments. The NMR spectra were assigned by the standard 2D spectroscopic methods of protein/peptide NMR [21]. Helicity profiles were determined primarily from chemical shift index (CSI) histograms. With the recent availability of three additional sets of coil values [22–24] in addition to our own [25], we have chosen to use the averages as the reference 'coil' values<sup>1</sup>. We assume that a 0.4 ppm or greater upfield shift for H $\alpha$  corresponds to a fully helical population at that residue.

For quantitative comparisons of medium range NOEs ( $i/i+n$ ,  $n = 2-4$ ), an additional set of TPPI-NOESY spectra were recorded (using a 3–9–19 'watergate' pulse sequence with a homospoil gradient pulse [26,27]) at 750 MHz ( $t_m = 170$  ms) for peptides  $U_1$  and  $U_5$  at 12 and 6 vol% TFE, respectively.

## 3. Results and discussion

In the fluoroalcohol-rich media (25% HFIP and/or 40% TFE), histograms of the H $\alpha$  chemical shift indices ( $\alpha$ CSIs) defined the helical domains of the amylin fragments lacking the disulfide linkage as Glu/Thr<sup>4</sup>  $\rightarrow$  Ser<sup>20</sup>, with C-terminal fraying, and as Ala<sup>5</sup>  $\rightarrow$  Ser<sup>20</sup> in the disulfide species [16]. At 25% HFIP, the H $\alpha$ -CSI histograms of  $U_1$  and  $U_0$  are essentially identical ( $\pm 0.03$  ppm) to those observed for full length amylin;  $U_5$  displays larger differences due to more extensive substitutions. The HN-CSI histograms at 25% HFIP are, however, less similar, with the (Aib)<sub>5</sub> species displaying a distinctly different set of downfield shifts suggesting some Aib-associated changes in the hydrogen bonding pattern.

Turning to the structural conclusion that can be drawn from NOE evidence, a <sup>15</sup>N-labelled amylin analog has been examined by 3D NMR; the <sup>15</sup>N-dispersed NOESY showed a continuous string of unambiguously assigned  $\alpha_i/N_{i+3}$  NOEs from  $i = 5 \rightarrow 21$  (Andersen and Liu, unpublished data). In 25% HFIP, the observed NOEs for peptides  $U_0$ ,  $U_1$  and  $U_5$  are also consistent with an  $\alpha$  helical conformation: for all instances where peaks are sufficiently resolved,  $i/i+3$  connectivities (either or both  $\alpha_i/N_{i+3}$  and  $\alpha_i/\beta_{i+3}$ ) appear from  $i = 5 \rightarrow 19$ ; and with two exceptions,  $\alpha_i/N_{i+2}$  NOEs are either entirely absent or significantly smaller than the corresponding  $\alpha_i/N_{i+4}$  NOEs. Those exceptions are: the cyclic species ( $U_0$ ) displays a 4 $\alpha$ /6N NOE, which appears to be a consistent consequence of the disulfide loop closure, both Aib<sup>7</sup> species display somewhat enhanced 6 $\alpha$ /8N NOEs. Peptide  $U_5$  does display a very weak 10 $\alpha$ /12N NOE. Overall it appears that, when the helix propagates well into the C-terminal portion of the sequence (at high levels of added fluoroalcohol), an  $\alpha$  helix forms even when portions of the sequence are Aib-rich.

In media without added fluoroalcohol, [Ser<sup>2,7</sup>]-hAM(1–20)GNH<sub>2</sub> and  $U_1$  display smaller upfield shifts (the maximum shift,  $-0.15$  ppm at Thr<sup>9</sup>, was observed for  $U_1$ ); upfield shifts are observed only over the Thr<sup>4</sup>  $\rightarrow$  Val<sup>17</sup> span indicating a more limited, and only partially populated, helix. The H $\alpha$  resonances of residues in the immediate vicinity of the Aib in  $U_1$  were shifted significantly upfield from their location in  $U_0$ . The CD ( $-\theta_{222} = 8790^\circ$  at 270 K) and NMR parameters for the (Aib)<sub>5</sub> mutant ( $U_5$ ) in aqueous buffer reveal a considerably more helical system with upfield  $\alpha$ CSI values of  $-0.18$  (Glu<sup>4</sup>),  $-0.37$  (Ser<sup>6</sup>),  $-0.35$  (Leu<sup>8</sup>),  $-0.30$  (Gln<sup>10</sup>),  $-0.20$  (Arg<sup>11</sup>),  $-0.11$  (Leu<sup>12</sup>),  $-0.41$  (Gln<sup>14</sup>),  $-0.27$  (Leu<sup>16</sup>), and  $-0.21$  (Val<sup>17</sup>). The less upfield shifts at residues 11–12 suggests a discontinuity in the helicity profile. Unambiguous NH<sub>*i*</sub>NH<sub>*i+1*</sub> connectivities are observed for  $i = 3, 5$ , and most of the sites surrounded by Aib residues; however, the NOESY spectrum did not provide (due to the lack of H $\alpha$  resonances for Aib, and insufficient dispersion of both backbone methyls and NHs) as many unambiguous through-space connectivities

<sup>1</sup> Since this set of reference values has not been published to date, it is given here for completeness using the one-letter code for residues, X (HN, H $\alpha$ ): A (8.21, 4.32), C (8.23, 4.57), C<sub>2</sub> (8.34, 4.69), D<sup>−</sup> (8.29, 4.65), D<sup>0</sup> or N (8.40, 4.72), E<sup>−</sup> (8.37, 4.32), E<sup>0</sup> or Q (8.27, 4.34), F (8.25, 4.61), G (8.28, 3.96), H<sup>+</sup> (8.35, 4.70), I (8.08, 4.15), K (8.19, 4.32), L (8.17, 4.32), M (8.25, 4.48), Nle (8.22, 4.32), P (−, 4.43), R (8.24, 4.34), S (8.26, 4.47), T (8.15, 4.37), U (8.08, −), V (8.08, 4.10), W (8.05, 4.65), and Y (8.13, 4.56 ppm). The values are for 25°C and a correction of  $-7.6$  ppb/°C [23] is applied to the HN reference values prior to determining the CSI from experimental data at other temperatures.

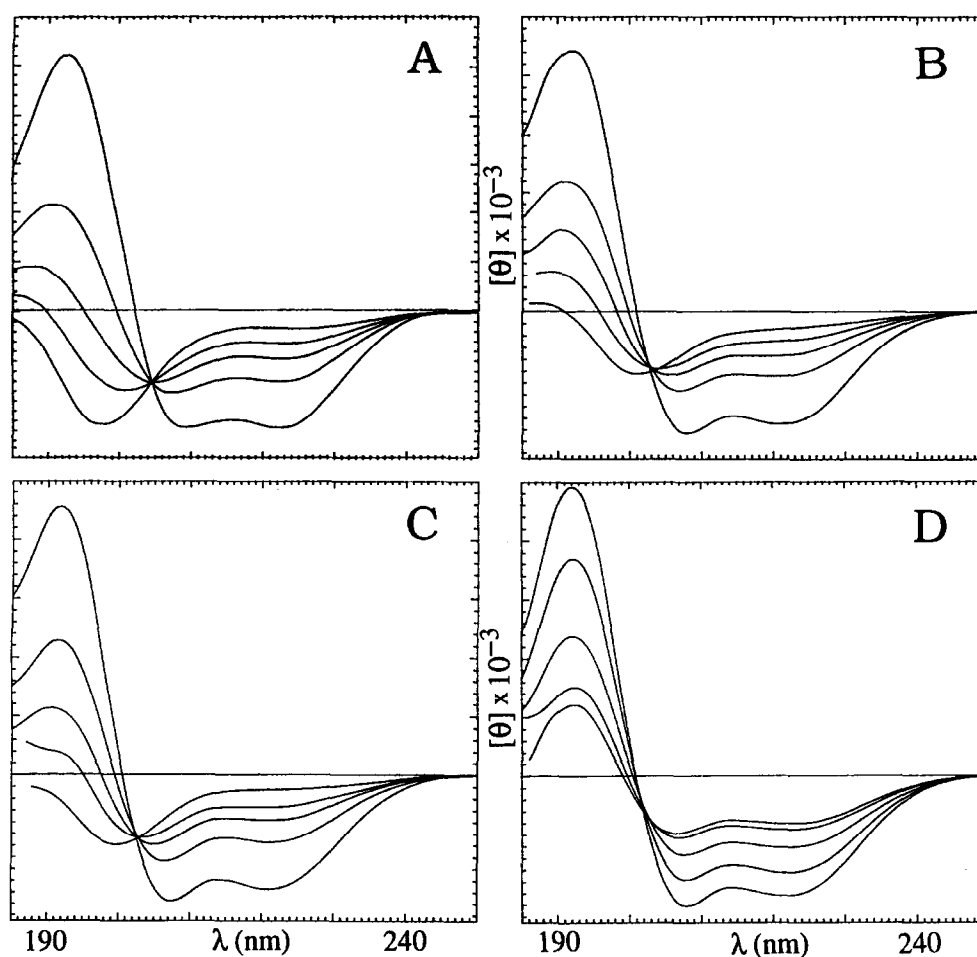


Fig. 1. A: Reference CD spectra for different levels of  $\alpha$  helix content; in order of increasing  $-\theta_{222}$  value the curves correspond to 10, 20, 30, 45 and 75% helix with the remaining portion being a slight modification of the 'disorder' spectrum of Yang et al. [1]. The other panels are spectra recorded for test peptides at 298 K at various levels of added TFE: B: peptide  $U_0$ , 0, 10, 13, 16 and 40%; C: peptide  $U_1$ , 0, 10, 13, 16 and 40%; D: peptide  $U_5$ , 0, 4, 8, 16 and 40% TFE.

as one would need for clear differentiation of  $3_{10}$  versus  $\alpha$  helical states. Peptide  $U_5$  was also examined in 2 vol% HFIP by CD ( $-\theta_{222} = 9870^\circ$  at 272 K) and NMR (at 300 K). The addition of this small amount of HFIP improves NH dispersion – strings of  $NH_iNH_{i+1}$  connectivities are observed for  $i = 3-9, 11-15,$  and  $17-20$  with those for residues  $i = 3, 9, 18, 19$  being relatively weak. Apparently, the diminished fractional helicity between the two Aib-rich segments observed in the absence of fluoroalcohol is quickly replaced by more extended helices as the HFIP content of the medium is increased. As a result, we aimed to obtain CD spectra for comparisons under conditions which corresponded to incomplete helix formation.

### 3.1. Circular dichroism spectra

In order to obtain CDs corresponding to different degrees of helicity, spectra were recorded for each peptide in aqueous buffer at pH 4.2 with the addition of fluoroalcohols, HFIP and TFE, to adjust the medium to any required composition in the range 2–40 vol% fluoroalcohol. This provided the CD curve shapes for the 188–250 nm span along the helix/coil transition for helices with differing Aib content. Peptides  $U_0$  and  $U_1$  displayed significant cold denaturation [28] in 4–8 vol% HFIP which precluded the generation of difference

CDs associated with thermal fraying that could be used to examine Aib substitution effects. Here, we focus on the TFE titration results which are collected in Fig. 1 together with the expectation curves for a random coil  $\rightarrow$   $\alpha$  helix transition (Fig. 1A). This CD study confirmed the greater helicity of  $U_5$  in the absence of added fluoroalcohol and a 'thermal fraying' study revealed unusual thermal stability:  $-\theta_{222} = 8790^\circ$  at 270 K, decreasing only slightly on warming;  $8080^\circ$  (at 298 K),  $6700^\circ$  (at 344 K)<sup>2</sup>. There were also distinctive differences in curve shape. Peptides  $U_0$  and  $U_1$  display  $[\theta]_{222}/[\theta]_{208}$  ratios (R2) at intermediate TFE levels that mimic the admixtures of  $\alpha$  helix and coil state reference spectra that appear in Fig. 1A, while  $U_5$  displays larger R2 values.

<sup>2</sup>We view the thermal behavior as strong evidence that  $U_5$  forms short Aib-nucleated helices rather than being a partially populated longer  $\alpha$  helix. The combined effect of thermal fraying and a TAS term favoring the random coil state would result in significant loss of the 222 nm band upon warming for a mixture of moderate length  $\alpha$  helices. In our opinion, at a comparable net fractional helicity, the helicity of peptides  $U_0$  and  $U_1$  is in larger part due to small populations of longer  $\alpha$  helices and the helical segments lacking an Aib melt and fray readily. NOE evidence that supports this view in the case of peptide  $U_5$  appears in a later section.

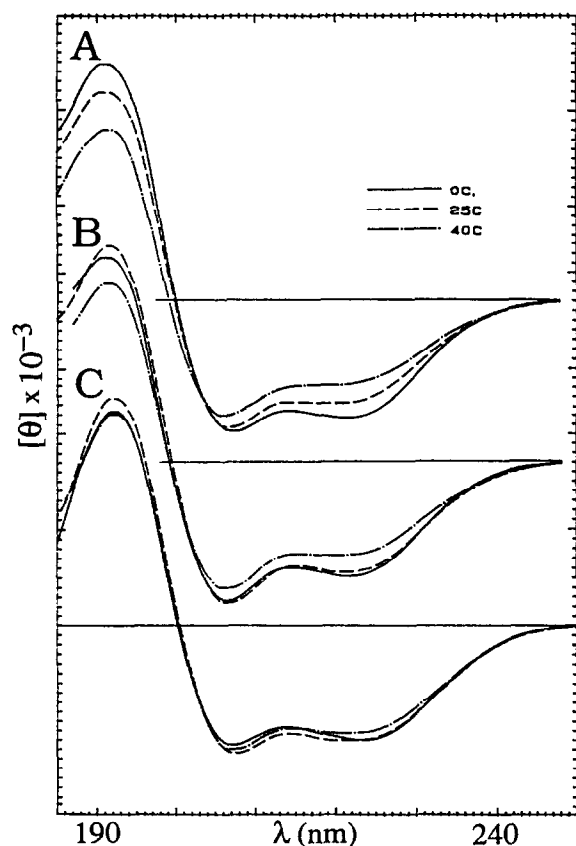


Fig. 2. The temperature dependence of CD spectra at an intermediate fractional helicity; solid line, 273 K; dashed line, 298 K; dot-dashed line, 313 K. A:  $U_0$  in 16% TFE; B:  $U_1$  in 16% TFE; C:  $U_5$  in 8% TFE. The tick marks on the  $[\theta]$  scale correspond to 1000<sup>3</sup>, the zero line is shown for each set of traces.

Peptides with no or one Aib residue reach approximately the same helicity as  $U_5$  in water (based on either the ellipticity at the  $n \rightarrow \pi^*$  band, the wavelength of the second minimum (205–205.6 nm), or the ellipticity at the maximum) at circa 13 vol% TFE. However, the curves are clearly not identical in shape, the  $(Aib)_5$  species displays a much smaller minimum at 206.6 nm. The temperature dependence of the CD traces were compared at a comparable stage in the TFE titration (8% TFE for  $U_5$ , versus 16% TFE for  $U_1$  and  $U_0$ , see Fig. 2). At this fluoroalcohol concentration as well, the  $(Aib)_5$  mutant appears to show no net unfolding upon warming<sup>3</sup>, only a slight shift in intensity from the  $n \rightarrow \pi^*$  band to the  $\pi \rightarrow \pi_{||}^*$  couplet was observed. Peptide  $U_0$  displays steady thermal melting, while  $U_1$  displays intermediate behavior: a curve shape change analogous to that of  $U_5$  from 273 to 298 K, and melting on further warming to 313 K. All of the changes were reversible and reproducible.

### 3.2. CD difference spectra

$\Delta$ CD spectra were employed to extract the differences in the curve shapes in helices with varying Aib content and to ascertain the corresponding spectral signatures for helix extension. Three types of experimental  $\Delta$ CD spectra were generated: (1)  $\Delta$ CDs due to fluoroalcohol-induced helix formation or extension, (2)  $[CD(Aib)_{x=n} - CD(Aib)_{x<n}]$  under solvent conditions

where the Aib-substituted peptides display enhanced helicity due to more favorable nucleation of short helices about Aib sites, and (3) the same differences with the fluoroalcohol content adjusted to give a comparable net % helicity for each analog. Representative  $\Delta$ CDs appear in Fig. 3. Fig. 3A shows the difference spectra for helix extension (from moderate helicity to that observed in 40% TFE). The  $\Delta$ CDs are very similar, with the  $(Aib)_5$  species displaying a somewhat smaller R2 value: 1.13 ( $U_0$ ), 1.09 ( $U_1$ ) and 0.968 ( $U_5$ ). This distinction is absent when the CD of the partially helical state of  $U_0$  is subtracted from the 40% TFE traces for all three peptides (Fig. 3B). It is tempting to conclude that, in the case of  $U_5$ , some  $3_{10}$  helical segments convert to an  $\alpha$  helical conformation at high fluoroalcohol levels.

Efforts to obtain the signatures of the helical form that is present at lower % helicity employed CD spectra with  $-[\theta]_{222}$  values equal or less than those seen in Fig. 2B. The low temperature spectra in Fig. 2B, which have nearly identical  $[\theta]_{222}$  values, were used to generate  $\Delta$ CDs by subtracting the spectrum of peptide  $U_0$  in the absence of TFE; the results appear as Fig. 3C. In Fig. 3D, the  $\Delta$ CDs associated with an even smaller degree of helicity are presented. To facilitate comparison, the  $\Delta$ CDs in panels C and D were normalized to the same  $\Delta[\theta]$  value at 222 nm.

The signatures (Fig. 3C,D) for the helicity present in the test systems at low % helicity are, in contrast to the signatures (Fig. 3A,B) for the added helicity that is introduced as the TFE content is increased to 40%, different for  $U_5$  and  $U_0$ : the  $\Delta$ CDs generated for  $U_5$  display a red shift for the  $n \rightarrow \pi^*$  band and have a reduced intensity  $\pi \rightarrow \pi^*$  couplet, particularly at the low energy  $\pi \rightarrow \pi_{||}^*$  band. The effect is most pronounced in Fig. 3D, less so in Fig. 3C for which the medium had been adjusted to 8% TFE for the spectrum of  $U_5$ . At low net helicity, the Aib-rich system displays a larger R2 value. Furthermore, if  $3_{10}$  helices are, indeed, characterized by a relatively diminished  $\pi \rightarrow \pi_{||}^*$  rotational strength; the TFE addition and thermal  $\Delta$ CDs suggest that some  $3_{10}$  segments convert to an  $\alpha$  helical conformation as TFE is added and upon warming in the 8% TFE medium.

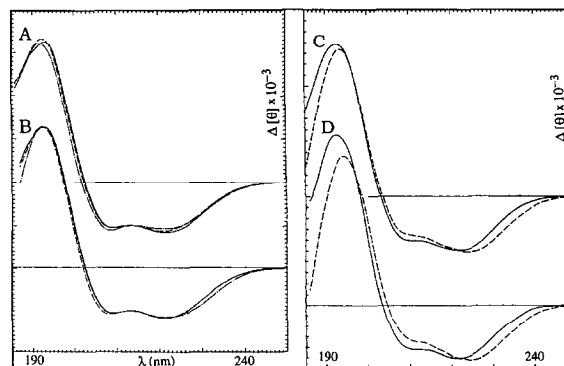


Fig. 3.  $\Delta$ CD spectra at 298 K unless otherwise specified. A: Solid line,  $U_0$  at 40% TFE minus  $U_0$  at 10% TFE; dashed line,  $U_1$  at 40% TFE minus  $U_1$  at 13% TFE; dot-dashed line,  $U_5$  at 40% TFE minus  $U_5$  at 0% TFE. B: Solid line,  $U_0$  at 40% TFE minus  $U_0$  at 10% TFE; dashed line,  $U_1$  at 40% TFE minus  $U_0$  at 10% TFE; dot-dashed line,  $U_5$  at 40% TFE minus  $U_0$  at 10% TFE. C (all traces at 273 K): solid line,  $U_0$  at 16% TFE minus  $U_0$  at 0% TFE; dashed line,  $U_5$  at 8% TFE minus  $U_0$  at 0% TFE. D: Solid line,  $U_0$  at 13% TFE minus  $U_0$  at 0% TFE; dashed line,  $U_5$  at 0% TFE minus  $U_0$  at 0% TFE.

<sup>3</sup> See footnote 1.

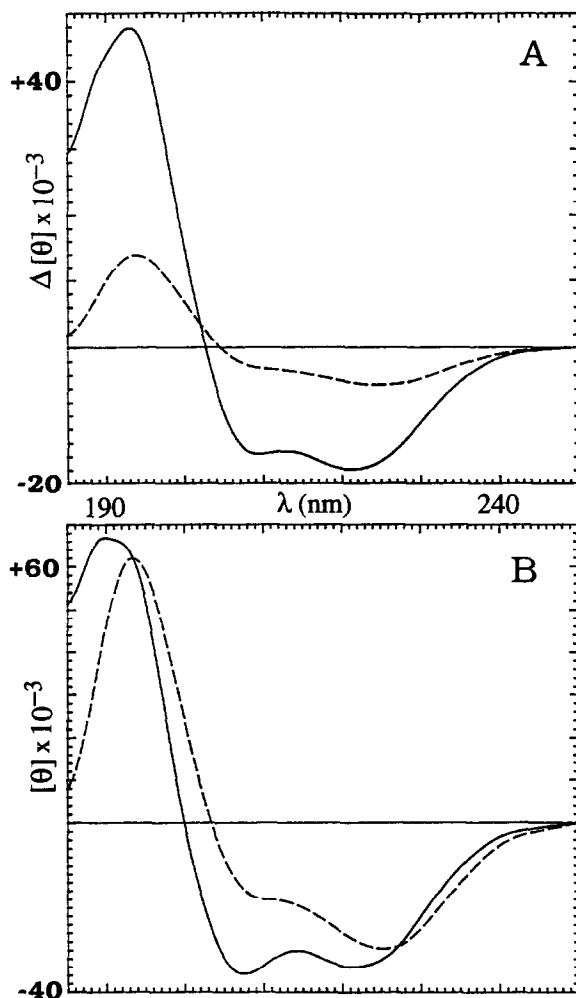


Fig. 4. Helicity difference spectra (A) and the helix signatures (B) derived therefrom. A (all traces at 273 K): Solid line,  $U_0$  at 40% TFE minus  $U_0$  at 0% TFE; dashed line,  $U_5$  at 0% TFE minus  $U_0$  at 0% TFE. B: Solid line, the CD signature of the helix in  $U_0$  at 40% TFE, normalized to  $-32000^\circ$  at the  $n \rightarrow \pi^*$  minimum; dashed line, the CD signature of the Aib-rich helix of  $U_5$  at 0% TFE, normalized to  $-28000^\circ$  at the  $n \rightarrow \pi^*$  minimum.

### 3.3. Confirmation of a $3_{10}$ to $\alpha$ helix transition provided by NOE observations

The CD studies presented in the previous section suggest that  $U_5$  is in the midst of a transition between two helical states between 4 and 8 vol% TFE. Although  $U_1$  in 12% TFE has the same 'net' helicity as  $U_5$  in 6% TFE (based on the ellipticity at 222 nm), to be consistent with our CD analysis the helical segments should be significantly different:  $U_1$  should display a lower population of a longer  $\alpha$  helix, while  $U_5$  should display characteristics of both  $3_{10}$  and  $\alpha$  helical segments. In principle, NOEs should distinguish these two 'states'; while both circumstances give rise to  $\alpha_i/\beta_{i+3}$  NOEs,  $3_{10}$  helices should display  $\alpha_i/N_{i+3}$  and  $\alpha_i/N_{i+2}$  NOEs and  $\alpha$  helices yield only  $\alpha_i/N_{i+3}$  and  $\alpha_i/N_{i+4}$  (the latter, in part through a secondary pathway [29],  $\alpha_i \rightarrow N_{i+3} \rightarrow N_{i+4}$ ). A secondary pathway for  $\alpha_i/N_{i+2}$  connectivities in frayed  $\alpha$  helices ( $\alpha_i \rightarrow N_{i+1} \rightarrow N_{i+2}$ ) also has been noted [30]; but it will always be accompanied by an  $\alpha_i/N_{i+1}$  NOE that is much larger than typical for a helical state.

The NOESY of  $U_1$  in 12% TFE displayed a  $12\alpha/16N$  peak

and the full set of  $\alpha_i/\beta_{i+3}$  and  $\alpha_i/N_{i+3}$  for  $i=6 \rightarrow 14$ , all of which were of somewhat diminished intensity (versus the  $\alpha_i/N_{i+1}$  NOEs) than the comparable spectrum in 25% HFIP. No  $\alpha_i/N_{i+2}$  NOEs were observed for  $U_1$  – the expected  $7\alpha Me/9N$  peaks is coincident with  $8\beta/9N$ ,  $6\alpha/8N$  is obscured, all the others are clearly absent. In striking contrast,  $U_5$  displays  $\alpha_i/N_{i+4}$  NOEs ( $i=8, 10, 11$  and  $12$  are unambiguous) and a wealth of  $\alpha_i/N_{i+2}$  and  $\alpha Me_i/N_{i+2}$  NOEs –  $i=3, 4, 5 Me, 6, 7 Me$  (ambiguous),  $9 Me, 10, 11, 12, 14$  (ambiguous) and  $15 Me$ . The  $i/i+2$  NOEs are typically of comparable intensity to the  $i+4$  NOEs and all  $\alpha_i/N_{i+1}$  NOEs were significantly smaller than the intra-residue  $\alpha N$  NOEs. Peptide  $U_5$  is, indeed, a mixture of  $\alpha$  and  $3_{10}$  helices under these conditions.

### 3.4. Deriving the CD signatures of short helices with and without Aib substitution

Difference spectra of the type shown in Fig. 3C,D provide a means for estimating the CD spectra of the short helices that are present in these peptides at a net helicity of 30–40%. In the case of  $U_5$ , the short helical segments should be predominantly in a  $3_{10}$  conformation. The difference spectra correspond to a fractional CD of the helix present less the corresponding fraction of random coil. Thus the spectrum of the short helix can be constructed by adding the appropriate amount of a random coil reference spectrum and renormalizing. For this, we employed the same coil spectrum employed for Fig. 1A and assumed that the short helices would display  $[\theta]_{222} = -28000^\circ + 120T^{(C)}$ . The specific  $\Delta CD$ s employed and the resulting helix signatures appear in Fig. 4. The same process was also applied to the 40% TFE versus water difference for  $U_0$  normalizing to  $[\theta]_{222} = -34000^\circ + 105T^{(C)}$ . The CD signature of the helix present in  $U_5$  in water displays the smallest 208 nm minimum and a red shifted  $n \rightarrow \pi^*$  peak. We attribute this to a short Aib-rich helix.

## 4. Conclusions

The present study has failed to confirm the conclusion of Millhauser [12] and Toniolo et al. [14] concerning the CD signature of  $3_{10}$  helices. Rather, we find that short helices are characterized by R2 values (the  $[\theta]_{222}/[\theta]_{208}$  ratio) greater than unity once the CD traces are corrected for the ellipticity contributions of disordered residues. This tendency is, if anything, enhanced in Aib-containing helices. The difference spectrum for helix formation associated with the addition of Aib residues displays a remarkable match to the  $\Delta CD$  associated with a pH-induced change in the helicity of hevein, a small globular protein containing one fluxional 5–8 residue helix [9]. Similar results have been obtained by inserting a proline residue at position 5 in RNase C-peptide analogs which limits the length of helix possible [8,10].

All of the difference spectra generated and the changes in the CD curves of the three test peptides during the TFE titration indicate that species with the short helices limited to Aib-rich segments have a relatively diminished rotational strength at the  $\pi \rightarrow \pi_{||}^*$  transition (207–208 nm). When titrated to a comparable net fractional helicity, the species lacking Aib residues appear to contain small populations of longer  $\alpha$  helices rather than well-populated short helical segments. In order for our data to be consistent with the previous suggestion [12,14] that  $3_{10}$  helices display R2 values much less than unity,  $U_5$  must form  $\alpha$  helices under all conditions examined. While

we cannot completely rule out the possibility that this (Aib)<sub>5</sub> species forms predominantly short  $\alpha$  helices, our NMR evidence is clearly to the contrary and, as a result, we urge extreme caution in applying the  $R2 < 1.0$  rule for identifying  $3_{10}$  helices. In the absence of additional evidence (ours will come from CD and NMR studies of U<sub>3R</sub> and U<sub>3G</sub>), we are inclined to concur with the Balam group [31] that “ $3_{10}$  and  $\alpha$  helices may not be distinguishable by CD”. Those differences that are present may simply reflect the fact that  $3_{10}$  helices are, of necessity, short helices. In addition, we note that the CD signature that we have generated for the  $3_{10}$  helix is, as might be expected based on the structural analogy, intermediate between that of an  $\alpha$  helix and that reported for type I/III turns [32].

NMR studies indicate that peptide U<sub>5</sub> undergoes a transition between two helical states both during a TFE titration and thermally at intermediate TFE levels. A detailed presentation of the NMR data will be published when the complete series of Aib mutants has been examined. Further studies of short helices are in progress.

*Acknowledgements:* The purchase of the 750 MHz NMR used in these studies was supported by the M.J. Murdock Charitable Trust and a grant from the National Science Foundation Academic Research Infrastructure Program.

## References

- [1] Yang, J.T., Wu, C.-S.C. and Martinez, H.M. (1986) *Methods Enzymol.* 130, 208–269.
- [2] Gans, P.J., Lyu, P.C., Manning, M.C., Woody, R.W. and Kalenbach, N.R. (1991) *Biopolymers* 31, 1606–1614.
- [3] Manning, M.C. and Woody, R.W. (1991) *Biopolymers* 31, 569–586.
- [4] Scholtz, J.M., Quian, H., York, E.J., Stewart, J.M. and Baldwin, R.L. (1991) *Biopolymers* 31, 1463–1470.
- [5] Woody, R.W. and Tinoco, I., Jr. (1967) *J. Chem. Phys.* 46, 4827–4845.
- [6] Madison, V. and Schellman, J.A. (1972) *Biopolymers* 11, 1041–1076.
- [7] Chen, Y.-H., Yang, J.T. and Chau, K.H. (1974) *Biochemistry* 13, 3350–3359.
- [8] Harris, S.M. (1993) Ph.D. Thesis, University of Washington, Seattle, WA.
- [9] Andersen, N.H., Cao, B., Rodríguez-Romero, A. and Arreguin, B. (1993) *Biochemistry* 32, 1407–1422.
- [10] Andersen, N.H., Harris, S.M., Lee, V.G., Liu, E., C.-K., Moreland, S. and Hunt, J.T. (1995) *BioOrg. Med. Chem.* 3, 113–124.
- [11] Andersen, N.H. and Palmer, R.B. (1994) *BioOrg. Med. Chem. Lett.* 4, 817–822.
- [12] Millhauser, G.L. (1995) *Biochemistry* 34, 3873–3877.
- [13] Bruch, M.D., Dhingra, M.M. and Gierasch, L.M. (1991) *Proteins Struct. Funct. Genet.* 10, 130–139.
- [14] Toniolo, C., Polese, A., Formaggio, F., Crisma, M. and Kamp-huis, J. (1996) *J. Am. Chem. Soc.* 118, 2744–2745.
- [15] Karle, I.L. and Balam, P. (1990) *Biochemistry* 29, 6747–6756.
- [16] Cort, J., Zhihong, L., Lee, G., Harris, S.M., Prickett, K.S., Gaeta, L.S.L. and Andersen, N.H. (1994) *Biochem. Biophys. Res. Commun.* 204, 1088–1095.
- [17] Liu, Z. and Andersen, N.H. (1995) 36th Experimental Nuclear Magnetic Resonance Conference, Boston, MA (3/95), Poster P-132.
- [18] Chakrabarty, A., Kortemme, T., Padmanabhan, S. and Baldwin, R.L. (1993) *Biochemistry* 32, 5560–5565.
- [19] Mihalyi, E. (1968) *J. Chem. Eng. Data* 13, 179–182.
- [20] Johnson, W.C., Jr. (1991) *Proteins Struct. Funct. Genet.* 7, 205–214.
- [21] Wüthrich, K. (1986) *NMR of Proteins and Nucleic Acids*, Wiley, New York.
- [22] Rico, M. and Nieto, J.L. (C.S.I.C., Madrid, Spain) provided a then current list of their  $\alpha$  methine reference values in a personal communication (1/95).
- [23] Merutka, G., Dyson, H.J. and Wright, P.E. (1995) *J. Biomol. NMR* 5, 14–24.
- [24] Wishart, D.S., Bigam, C.G., Holm, A., Hodges, R.S. and Sykes, B.D. (1995) *J. Biomol. NMR* 5, 67–81.
- [25] Andersen, N.H., Chen, C. and Lee, G.M. (1995) *Protein Peptide Lett.* 1, 215–222.
- [26] Piotto, M., Saudek, V. and Sklenar, V. (1992) *J. Biomol. NMR* 2, 661–666.
- [27] Sklenar, V., Piotto, M., Leppik, R. and Saudek, V. (1993) *J. Magn. Reson. Ser. A* 102, 241–245.
- [28] Andersen, N.H., Cort, J.R., Liu, Z., Sjöberg, S.J. and Tong, H. (1996) *J. Am. Chem. Soc.* 118, in press.
- [29] Bruch, M.D., McKnight, C.J. and Gierasch, L.M. (1989) *Biochemistry* 28, 8554–8561.
- [30] Andersen, N.H., Chen, C., Marschner, T.M., Krystek, S.R., Jr. and Bassolino, D.A. (1992) *Biochemistry* 31, 1280–1295.
- [31] Sudha, T.S., Vijayakumar, E.K.S. and Balam, P. (1983) *Int. J. Pept. Protein Res.* 22, 464–468.
- [32] Perczel, A. and Fasman, G.D. (1992) *Protein Sci.* 1, 378–395.